nature structural & molecular biology

A novel actin binding site of myosin required for effective muscle contraction

Boglárka H Várkuti[1,7], Zhenhui Yang[1,7], Bálint Kintses[1,2], Péter Erdélyi[3], Irén Bárdos-Nagy[4], Attila L Kovács[5], Péter Hári[6], Miklós Kellermayer[4], Tibor Vellai[3] & András Málnási-Csizmadia[1]

F-actin serves as a track for myosin's motor functions and activates its ATPase activity by several orders of magnitude, enabling actomyosin to produce effective force against load. Although actin activation is a ubiquitous property of all myosin isoforms, the molecular mechanism and physiological role of this activation are unclear. Here we describe a conserved actin-binding region of myosin named the 'activation loop', which interacts with the N-terminal segment of actin. We demonstrate by biochemical, biophysical and *in vivo* approaches using transgenic *Caenorhabditis elegans* strains that the interaction between the activation loop and actin accelerates the movement of the relay, stimulating myosin's ATPase activity. This interaction results in efficient force generation, but it is not essential for the unloaded motility. We conclude that the binding of actin to myosin's activation loop specifically increases the ratio of mechanically productive to futile myosin heads, leading to efficient muscle contraction.

Several cellular motor functions, including cell proliferation and differentiation, muscle contraction and intracellular transport, are powered by different types of myosins, which act in complex with actin[1,2]. Myosins (**Fig. 1a**) constitute a diverse protein family (currently grouped at least into 35 classes) and are ubiquitous in all eukaryotic cells[3]. Despite the large functional variety of myosins, there is a universal fundamental molecular mechanism underlying the actomyosin chemomechanical cycle. The cyclic actin binding and release alternating with the swing and structural relaxation of the myosin lever define the mechanical cycle of actomyosin that is coupled with the chemical cycle, including the nucleotide binding, hydrolysis and product release steps. After a rapid ATP-induced actin dissociation and the recovery swing of the lever, ATP hydrolysis occurs in the lever-up state[4]. Rebinding of actin to this myosin after this hydrolytic state of myosin induces the up-to-down lever swing, also known as the powerstroke (**Fig. 1b**,**c**). The efficiency of the actomyosin cycles depends on the ratio of the reaction fluxes of the actin-attached to the actin-detached up-to-down lever swings (the ratio of productive to futile pathways, respectively) (**Fig. 1c**). Recent results showed that in the absence of actin, the rate-limiting step of the ATPase cycle is not the phosphate release but, rather, is the preceding lever swing[5]. Actin accelerates the steady-state ATPase activity of myosin (known as actin activation) by increasing the rate constant of the lever swing, thereby channeling the enzymatic system toward the effective chemomechanical pathways (**Fig. 1d**). This mechanistic model suggests that the ratio of the productive to futile cycles is regulated by the allosteric activation of the lever swing by actin[6]. In the absence of actin activation, however, motility and contraction may still occur, being driven by occasional strokes of the myosin lever in the actin-bound form. Considering the efficiency of the system, at low actin activation, myosin heads usually hydrolyze ATP without an effective lever swing (a low ratio of effective cycles to hydrolyzed ATP), whereas at high actin activation, most heads are channeled to the effective pathway (a high ratio of effective cycles to hydrolyzed ATP). Consequently, the lack of actin activation in a muscle fiber would result in a low work production and, hence, mechanical weakness of contraction.

The pivotal question is, what is the molecular mechanism behind actin activation of myosin that determines the force and velocity of muscle contraction? The importance of understanding the actin activation of myosin extends beyond muscle function. This process probably resembles the activation of a wide array of NTPases by their own track system or activator. In support of this notion is the fact that allosteric activation is an evolutionarily conserved universal mechanism among motor proteins and signaling enzyme complexes, including kinesin–tubulin, G protein–guanine nucleotide exchange factor[7] and kinase–scaffold systems[8]. Although the phenomenon of actin activation has long been acknowledged, its mechanism and structural background are unknown. We believe that this process is related to a specific actin-myosin interaction.

The atomic structure of actomyosin has not been determined, however, high resolution electron micrography[9,10] and *in silico* docking simulations[11–14] showed that the spacious interface of rigor actomyosin is separated by a deep cleft that is surrounded by the upper and lower actin binding subdomains of myosin (**Fig. 1e**). The closure of this cleft increases the strength of the actin binding[15]. The loops of

[1]Department of Biochemistry, Eötvös Loránd University, Budapest, Hungary. [2]Department of Biochemistry, University of Cambridge, Cambridge, UK. [3]Department of Genetics, Eötvös Loránd University, Budapest, Hungary. [4]Department of Biophysics and Radiation Biology, Semmelweis University, Budapest, Hungary. [5]Department of Anatomy, Cell and Developmental Biology, Eötvös Loránd University, Budapest, Hungary. [6]Delta Informatika, Budapest, Hungary. [7]These authors contributed equally to this work. Correspondence should be addressed to A.M.-C. (malna@elte.hu).

Received 14 January 2011; accepted 29 November 2011; published online 12 February 2012; doi:10.1038/nsmb.2216

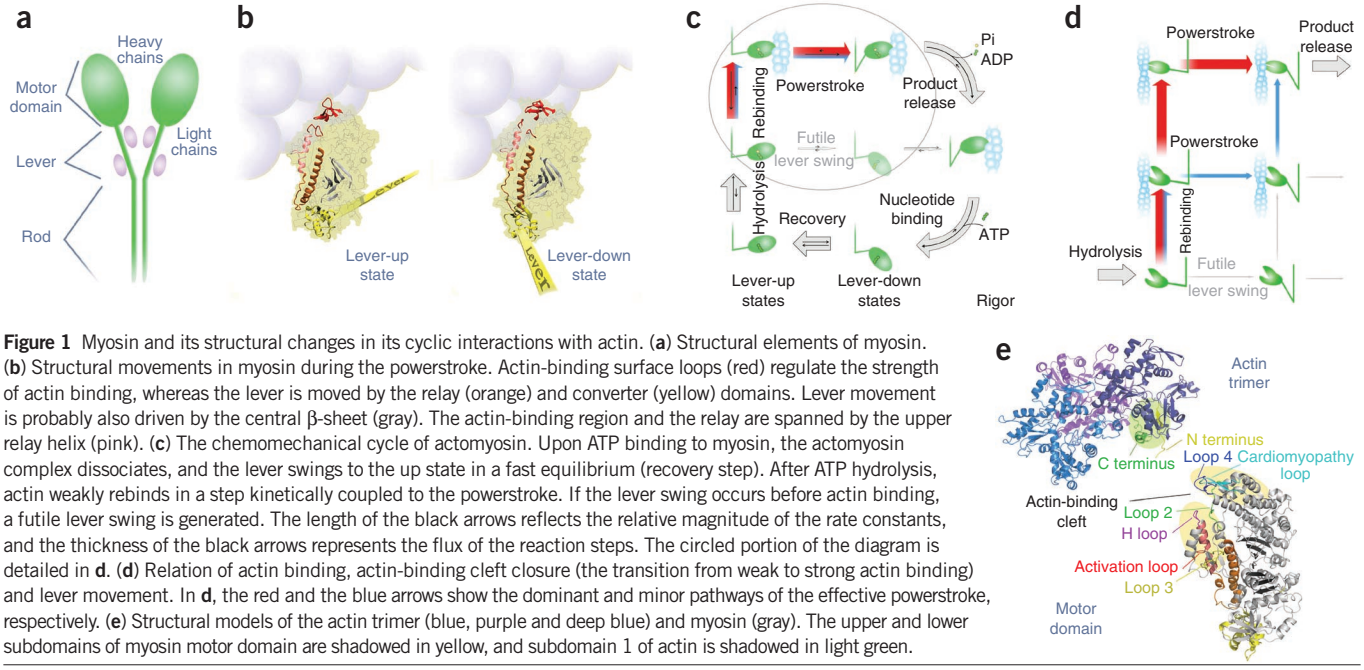

Figure 1 Myosin and its structural changes in its cyclic interactions with actin. (**a**) Structural elements of myosin. (**b**) Structural movements in myosin during the powerstroke. Actin-binding surface loops (red) regulate the strength of actin binding, whereas the lever is moved by the relay (orange) and converter (yellow) domains. Lever movement is probably also driven by the central β-sheet (gray). The actin-binding region and the relay are spanned by the upper relay helix (pink). (**c**) The chemomechanical cycle of actomyosin. Upon ATP binding to myosin, the actomyosin complex dissociates, and the lever swings to the up state in a fast equilibrium (recovery step). After ATP hydrolysis, actin weakly rebinds in a step kinetically coupled to the powerstroke. If the lever swing occurs before actin binding, a futile lever swing is generated. The length of the black arrows reflects the relative magnitude of the rate constants, and the thickness of the black arrows represents the flux of the reaction steps. The circled portion of the diagram is detailed in **d**. (**d**) Relation of actin binding, actin-binding cleft closure (the transition from weak to strong actin binding) and lever movement. In **d**, the red and the blue arrows show the dominant and minor pathways of the effective powerstroke, respectively. (**e**) Structural models of the actin trimer (blue, purple and deep blue) and myosin (gray). The upper and lower subdomains of myosin motor domain are shadowed in yellow, and subdomain 1 of actin is shadowed in light green.

the upper subdomain bind actin only in the strong actin-binding state[16,17], whereas the lower subdomain interacts with actin in both the strong and weak actin-binding states of myosin. Mutations in the actin-binding loops of the lower subdomain reduced both actin activation and the motility of myosin (by affecting both the weak and strong actin-binding states)[18–21]. These papers concluded that motility and actin activation are mechanistically coupled and might be directly related to the cleft closure of the actin-binding site. By contrast, the mechanistic model described above (**Fig. 1c**,**d**) suggests that motility may occur without the actin activation of myosin[6]. A further consequence of the model is that actin activation cannot be controlled directly by the cleft closure because the powerstroke is initiated before this process takes place (**Fig. 1d**). The first experimental indication for uncoupling actin activation from motility was that mutations of the conserved, negatively charged N-terminal segment of actin suppressed its ability to activate myosin ATPase while retaining *in vitro* motility[22] in complex with myosin. However, finding the element of myosin that interacts with this actin segment was hindered by the fact that the atomic structure is undetermined in the existing structural models of actomyosin[11,12].

To unravel the structural details of actomyosin interactions, molecular mechanisms of actin activation and their influence on mechanical performance, we (i) remodeled the actomyosin complex in weak and strong actin-binding states, including the N-terminal segment of actin, and identified a new actin-binding loop of myosin; (ii) revealed experimentally the specific role of this loop in actin's activation of myosin ATPase; and (iii) tested the *in vivo* role of actin activation in muscle contraction in transgenic *C. elegans* worms.

RESULTS

Uncovering a novel actomyosin interaction site

The highly flexible, evolutionary conserved, negatively charged N-terminal region of actin seems to be crucial to the actin-myosin interaction during the pre-powerstroke (lever-up) state of myosin[22,23], however, the structure and function of this region are not known. To explore the interactions of this actin region with myosin, we constructed new *in silico* structural models of actomyosin in strong and weak actin-binding states, including both the up- and down-lever myosin states. The actin subunits were extended by the missing N-terminal segment (1-Asp-Glu-Asp-Glu-4), which included the acetylation of the N terminus as well (**Fig. 2**). We found that in all three states (rigor complex, weak actomyosin binding with lever-up complex and weak actomyosin with lever-down complex), the negatively charged N-terminal peptide of actin forms a salt bridge cluster with Arg520 or its homolog, Lys528 (for *Dictyostelium discoideum* and squid motor-domain sequence numbering, respectively) of the myosin motor domain. This arginine or lysine is located in a small loop of the upper relay helix, which we named the activation loop. The formation of the salt bridge was spontaneous even in the first, docking phase and remained stable during the entire running of the molecular dynamics simulations. Based on sequence comparison, the 5- to 10-residue-long activation loop exists in all myosin isoforms. The activation loop always contains a positively charged residue in the same position in all isoforms (**Supplementary Fig. 1a**). This amino acid side chain points toward the solution in all the available myosin structures and therefore its interaction with any other side chain of myosin is highly unlikely.

To obtain direct experimental evidence for the specific interaction between actin and myosin's activation loop, we conducted covalent actomyosin cross-linking experiments using a zero-length cross-linker, 1-ethyl-3-(3-dimethylaminopropyl)carbodiimide (EDC), which creates cross-links between the proximal lysine and aspartate or glutamate side chains. When the *D. discoideum* motor domain was cross-linked with actin by EDC, we detected only one cross-linked product using SDS-PAGE (labeled MD_{wt} in **Fig. 3a**). When we replaced Arg520 of *D. discoideum* myosin with a lysine, we detected two specific, cross-linked actomyosin products, one with a higher molecular mass and one with a lower molecular mass (labeled MD_{R520K} in **Fig. 3a**). This result is similar to those found in previous experiments using rabbit skeletal-muscle myosin, in which, at the position homologous to Arg520, a lysine exists[24,25]. In these previous studies, the actomyosin product of lower molecular mass was determined to be a covalent crosslink between loop 2 of myosin and domain 1 of actin[25], whereas the crosslink position of the actomyosin

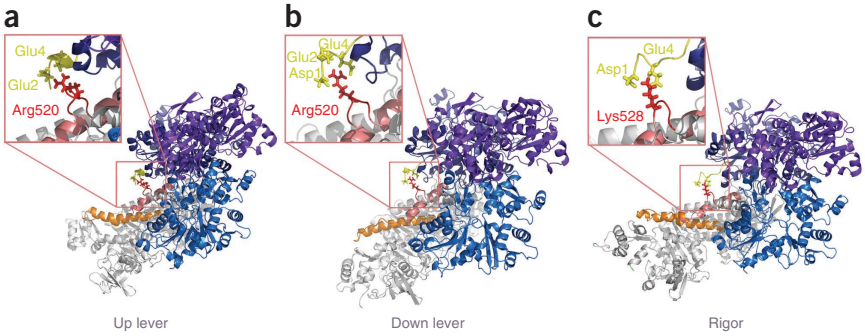

Figure 2 Interactions between the activation loop and the N-terminal segment of actin in three states of actomyosin obtained from molecular dynamics simulations. (**a**–**c**) Structural models of actomyosin in the up-lever, weak (**a**), down-lever, weak (**b**) and strong (**c**) actin-binding states of the *D. discoideum* myo-2 and squid motor domains. The initial actin structure used in these simulations was restored by the originally missing, negatively charged four-amino acid N-terminal segment (yellow), which forms a salt bridge cluster with the conserved positively charged amino acid of the activation loop (red) of myosin, located in the upper relay region (pink). This interaction is enlarged in the inset boxes.

product of higher molecular mass was ambiguous[26]. In our experiments, a single arginine to lysine mutation at position 520 of the *D. discoideum* motor domain provided the actomyosin adduct of higher molecular mass, indicating that residue 520 contacts the N-terminal carboxyl side chains of actin. The cross-linking reactions proceeded to the same extent in all studied conditions, each of which represented a different conformational state of myosin: the lever-up state (in the presence of ATPN, a non-hydrolysable ATP analog[27,28]), the lever-down state (in the presence of ADP) and rigor (in the absence of nucleotide) (data not shown). We conclude that the interaction of the activation loop with actin is stable in all conformational states of the myosin motor domain, which is consistent with the results of our molecular dynamics simulations described above.

Role of myosin's activation loop in actin binding

We produced a series of *D. discoideum* myosin 2 motor domain constructs with mutations in their activation loops to selectively suppress the interaction between the activation loop and the N-terminal peptide of actin. First, we designed and expressed a mutant of the *D. discoideum* myosin motor domain in which we deleted the activation loop by removing all amino acids of the (519-Gly-Arg-Gln-Pro-Pro-523) loop. Based on structural simulations, we predicted that the upper relay helix of the activation-loop–deleted mutant would become a continuous helical structure (**Supplementary Fig. 1c**). In other constructs, we mutated Arg520 to either a neutral glutamine or a negatively charged glutamate. To test the validity of our model for processive myosins, we constructed a mutant

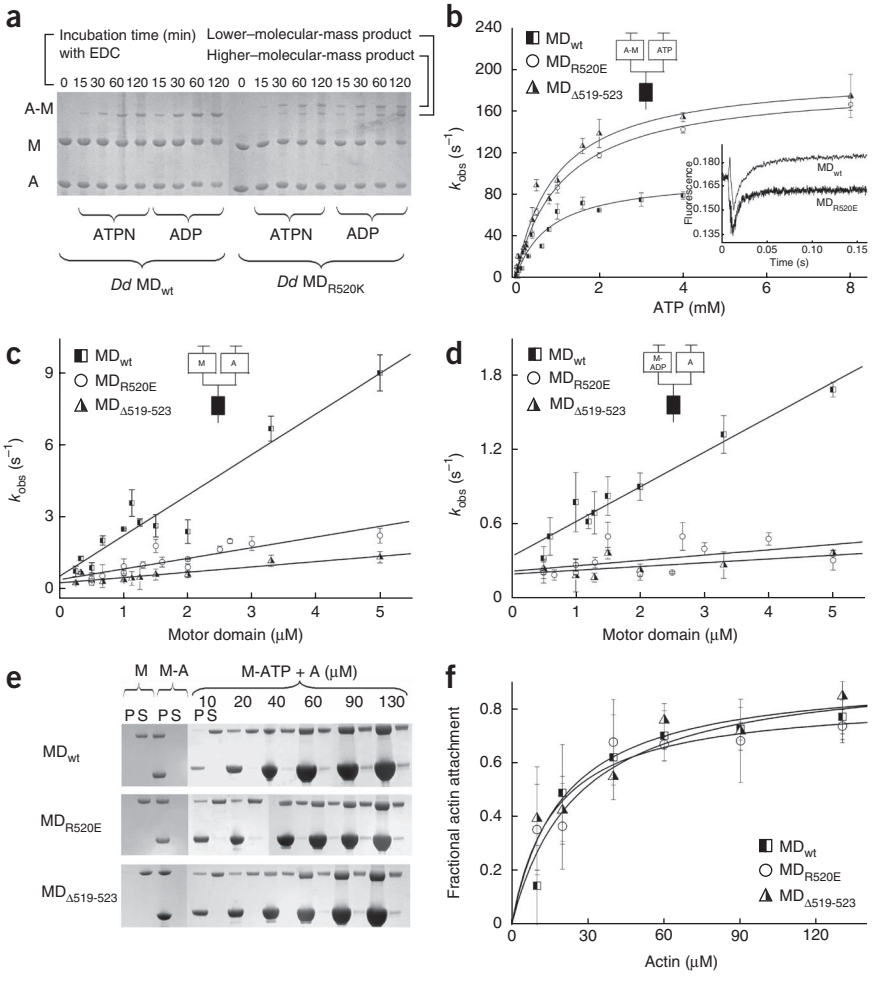

Figure 3 Actin-binding properties of wild-type and mutant *D. discoideum* (*Dd*) myosin motor domain (MD). (**a**) SDS-PAGE visualizing zero-length cross-linking. Actin (A) and wild-type or R520K mutant *D. discoideum* myosin motor domains (M) were mixed with ADP or ATPN and cross-linked to form actomyosin complexes (A-M). (**b**) ATP-induced actin dissociation from wild-type motor domains (MD_{wt}) and mutant motor domains (with the R520E mutation (MD_{R520E}) or the activation loop deletion ($MD_{\Delta519\text{-}523}$)) as a function of increasing ATP concentration followed by stopped flow. The inset shows that the motor domain and pyrene-labeled F-actin were mixed with Mg-ATP, and the pyrene fluorescence increase was monitored (**Table 1**). For all stopped-flow experiments, the small diagrams depict the components of the rapid mixes, and the data points represent the means of at least three independent experiments ± s.d. (**c**,**d**) The observed rate constants of the binding of wild-type motor domains and two mutant motor domains to pyrene-labeled F-actin as a function of motor domain concentration in the absence (**c**) and presence (**d**) of Mg-ADP (**Table 1**). (**e**) Actin co-sedimentation assays of wild-type motor domains and two mutant motor domains. Pellets (P) and supernatants (S) from mixtures of myosin motor domains in the presence of ATP (M-ATP) with increasing concentrations of actin (A) were visualized on Coomassie brilliant blue–stained SDS gels. Myosin alone (M) and actomyosin in the absence of ATP (M-A) are shown as controls. (**f**) Fractional actin attachments of wild-type motor domains and two mutant motor domains were determined by the densitometry of the SDS gels in **e**. See also **Table 1**.

Table 1 Nucleotide- and actin-binding properties of wild-type and mutant *D. discoideum* motor domains

Nucleotide-binding properties—rate and equilibrium constants in the absence of actin

	ADP binding[a]			ATP binding[b]	ATP hydrolysis[b]
	k_{on} (s^{-1} μM^{-1})	k_{off} (s^{-1})	K_d (μM)	k_{on} (s^{-1} μM^{-1})	$k_{hydrolysis}$ (s^{-1})
D. discoideum MD_{wt}	0.7 ± 0.14	7.2 ± 1.5	10.1 ± 3.0	1.2 ± 0.02	31 ± 1.2
D. discoideum MD_{R520E}	0.69 ± 0.12	7.6 ± 2.1	10.9 ± 3.6	1.2 ± 0.02	34 ± 0.8
D. discoideum $MD_{\Delta 519\text{-}523}$	0.90 ± 0.22	7.1 ± 4.2	7.8 ± 5.0	1.3 ± 0.02	**18 ± 1.4**

Actin-binding properties—rate and equilibrium constants in the absence or presence of nucleotides

	Actin binding in the apo state[c]			Actin binding in the ADP-bound state[c]			Actin binding in the presence of ATP	Actomyosin dissociation by ATP[c]
	k_{on} (s^{-1} μM^{-1})	k_{off} (s^{-1})	$K_{d,apo}$ (μM)	k_{on} (s^{-1} μM^{-1})	k_{off} (s^{-1})	$K_{d,ADP}$ (μM)	$K_{d,ATP}$ (μM)	$k_{actin\ dissoc}$ (s^{-1})
D. discoideum MD_{wt}	1.7 ± 0.16	0.54 ± 0.33	0.32 ± 0.21	0.28 ± 0.02	0.34 ± 0.05	1.2 ± 0.26	26 ± 9.7	97 ± 8
D. discoideum MD_{R520E}	**0.40 ± 0.16**	0.44 ± 0.07	**1.1 ± 0.61**	**0.043 ± 0.02**	0.22 ± 0.05	**5.2 ± 2.3**	17 ± 5.7	**186 ± 4**
D. discoideum $MD_{\Delta 519\text{-}523}$	**0.22 ± 0.03**	0.27 ± 0.07	**1.2 ± 0.46**	**0.030 ± 0.02**	**0.20 ± 0.05**	6.5 ± 6.0	20 ± 6.8	**195 ± 11**

The means ± s.d. of the rate constants are shown and were determined from at least three independent experiments using the stopped-flow transient kinetic method, which detects changes in fluorescence. K_d values were calculated from the appropriate rate constants, except for $K_{d,ATP}$, which was determined from fitting the hyperbola to the data. For detailed data analyses, see **Supplementary Methods**. Values in bold are significantly different from that of the wild type ($P < 0.05$).
[a]Mant-dADP fluorescence. [b]Tryptophan fluorescence. [c]Pyrene-actin fluorescence.

with the K502E mutation in the myosin 5 head domain (S1) (using *Mus musculus* dilute numbering, this position is an analog to Arg520 in *D. discoideum* myosin).

We carried out a thorough kinetic characterization of the *D. discoideum* motor domain mutants in the absence of actin and compared the results with those obtained for the wild type. We investigated ATP- and ADP-binding properties, lever recovery, hydrolysis steps and ADP release using stopped-flow methods. We detected no statistically significant difference between the wild-type[29] and mutant forms in any of the kinetic steps (**Table 1**). Even the steady-state ATPase (Mg-ATPase) activity was unchanged by the mutations in the absence of actin. The actin-binding properties of the mutants slightly differed from those of the wild type (**Fig. 3b–f**).

In the absence of nucleotides and in the presence of ADP, the K_d of actomyosin of the activation loop mutants increased approximately five-fold compared to those states of the wild type (**Fig. 3c**,**d** and **Table 1**). Consequently, the coupling ratio of actin binding in the apo and ADP forms of the mutants ($K_{d,apo}/K_{d,ADP}$) did not change compared to the wild type. We found a small increase in the rate constant of the ATP-induced actin dissociation ($k_{actin\ dissoc}$) (**Fig. 3b** and **Table 1**). In the presence of ATP, the interactions of the mutants with actin were as weak as those of the wild type ($K_{d,\ ATP}$) (**Fig. 3e**,**f** and **Table 1**). All kinetic perturbations caused by mutations of the activation loop were associated with actin binding, providing further evidence for the existence of interaction between myosin's activation loop and actin.

Uncoupling of actin activation and motility

F-actin increases the basal steady-state Mg-ATPase activity of the wild-type *D. discoideum* motor domain by almost two orders of magnitude by actin activation. Notably, the basal steady-state Mg-ATPase activities of the activation-loop mutants were elevated only two-fold to four-fold, even at very high concentrations of actin (**Fig. 4a** and **Table 2**), and we observed a similar effect for the *M. musculus* myosin 5 S1 (**Fig. 4b**). These results indicate that the activation loop is specifically responsible for actin activation of the myosin ATPase cycle.

As unloaded muscle contraction can proceed even at very low duty ratios, our mechanistic model predicted that a lack of actin activation does not hinder the sliding motion of myosin along the actin filament. We note that the velocity of the motility is not determined by the steady-state ATPase activity, as it was previously shown to be controlled by the rate of the actin detachment after the power-stroke in *D. discoideum* myosin[30–32]. However, we note that actin activation and the velocity of filament movement, depending on the myosin isoforms, could be limited by different steps, that include a hydrolysis step[33,34], the actin affinities in different myosin states and ADP release[35,36] (for a more detailed discussion, see **Supplementary Discussion**). To test whether activation-loop–specific mutations indeed leave myosin-driven unloaded contraction intact, we carried out *in vitro* motility assays using mutant myosins and wild-type myosins. The average filament sliding speed for the wild-type motor domain was similar to that reported previously[37]. The filament velocities for the activation-loop–mutant motor domain constructs were also very similar to that of the wild-type construct (**Fig. 4c** and

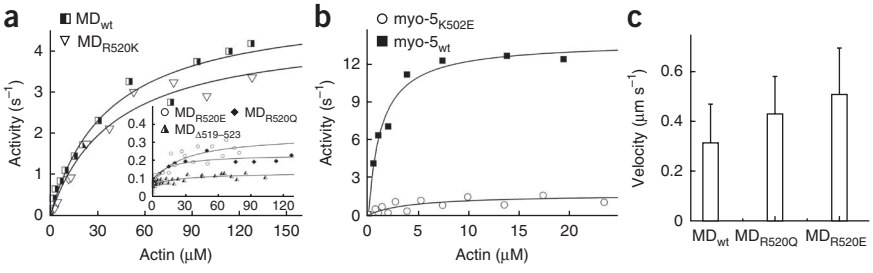

Figure 4 Mutations in the activation loop of myosin suppress actin activation, whereas *in vitro* motility function is unaffected. (**a**) Steady-state actin-activated ATPase activities of wild-type (MD_{wt}) and mutant *D. discoideum* myosin 2 motor domains as a function of actin concentration. The inset shows MD_{R520Q}, MD_{R520E} and $MD_{\Delta 519\text{-}523}$ in a *y*-axis–upscaled graph to show the saturation of their ATPase activities. (**b**) Steady-state actin-activated ATPase activities of wild-type (myo-5_{wt}) and activation-loop mutant (with the K502E mutation (myo-5_{K502E})) *M. musculus* myosin 5 S1 as a function of actin concentration (**Table 2**). (**c**) *In vitro* motilities of wild-type and mutant *D. discoideum* motor domain constructs. Error bars, s.d. of at least three independent experiments (**Table 2**).

Table 2 Basal- and actin-activated ATPase activity and *in vitro* motility sliding speed of *D. discoideum* motor domain and myo 5 S1 constructs

	Activities				Sliding speeds
	V_{basal}[a] (s^{-1})	V_{max}[b] (s^{-1})	K_{actin}[b] (μM)	Acceleration	v (μm s^{-1})
D. discoideum MD_{wt}	0.067 ± 0.011	5.1 ± 0.37	36.9 ± 7.0	66×	0.32 ± 0.15
D. discoideum MD_{R520Q}	0.070 ± 0.014	0.15 ± 0.01	13.3 ± 5.0	1.9×	0.43 ± 0.15
D. discoideum MD_{R520E}	0.068 ± 0.013	0.27 ± 0.05	26.8 ± 14.0	3.5×	0.51 ± 0.18
D. discoideum $MD_{Δ519-523}$	0.064 ± 0.010	0.13 ± 0.01	26.6 ± 14.0	1.8×	
D. discoideum MD_{R520K}	0.070 ± 0.017	4.5 ± 0.38	39.8 ± 8.3	52×	
M. musculus myo-5_{wt}	0.038 ± 0.004	13.8 ± 0.59	1.3 ± 0.2	690×	
M. musculus myo-5_{K502E}	0.029 ± 0.011	1.6 ± 0.33	4.4 ± 2.7	76×	

The means ± s.d. of all the parameters are shown and were determined from three independent experiments. V_{basal}, basal ATPase activity (no actin); V_{max}, maximal actin-activated ATPase activity; K_{actin}, actin concentration at half of V_{max}; v, velocity.
[a]Determined from NADH-coupled assay. [b]Determined from hyperbola fitted to data of coupled assay.

Table 2). Notably, for the mutant constructs, the coverslip had to be coated with myosin at about a ten-fold higher concentration relative to the wild-type construct to evoke motion.

The results of the kinetic and *in vitro* motility assays show that actin activation and motility can be uncoupled by blocking the interaction between myosin's activation loop and actin's N-terminal region. The finding that a more dense myosin field is required for the effective motility of activation-loop mutants than the wild-type motor domain is consistent with the mechanistic model, as actin activation channels the cycles toward the effective powerstroke, increasing the probability of such an event. Notably, without actin activation, only the magnitudes of the binding constant and the actin concentration determine the frequency of the effective powerstrokes. As the binding constant of actomyosin is low at this step in the cycle, the frequency of effective powerstrokes is correspondingly low. However, as a result of the unloaded conditions, actin filaments are propelled forth with unchanged sliding speed even at a reduced temporal frequency of effective myosin heads, provided that their spatial frequency is increased. Thus, in an *in vitro* motility assay, a denser activation-loop–mutant myosin field is able to move actin filaments with speeds identical to that of the wild-type myosin field. In summary, the magnitude of actin activation determines the ratio of effective to futile ATPase cycles of myosin.

In vivo role of the activation loop

Because of the high specificity of the mutations in the activation loop, the process of actin activation may be singularly explored *in vivo* by using a transgenic model system. We designed and generated transgenic *C. elegans* strains in which we introduced a mutation in the activation loop of the body-wall muscle myosin UNC-54. We investigated changes in muscular physiology evoked by the alleviation of actin activation by measuring the motile features and mechanical properties of these worms in new experimental assays.

Four different types of genes coding for myosin 2 exist in *C. elegans*: *myo-1* and *myo-2* are expressed only in the pharynx, and *myo-3* and

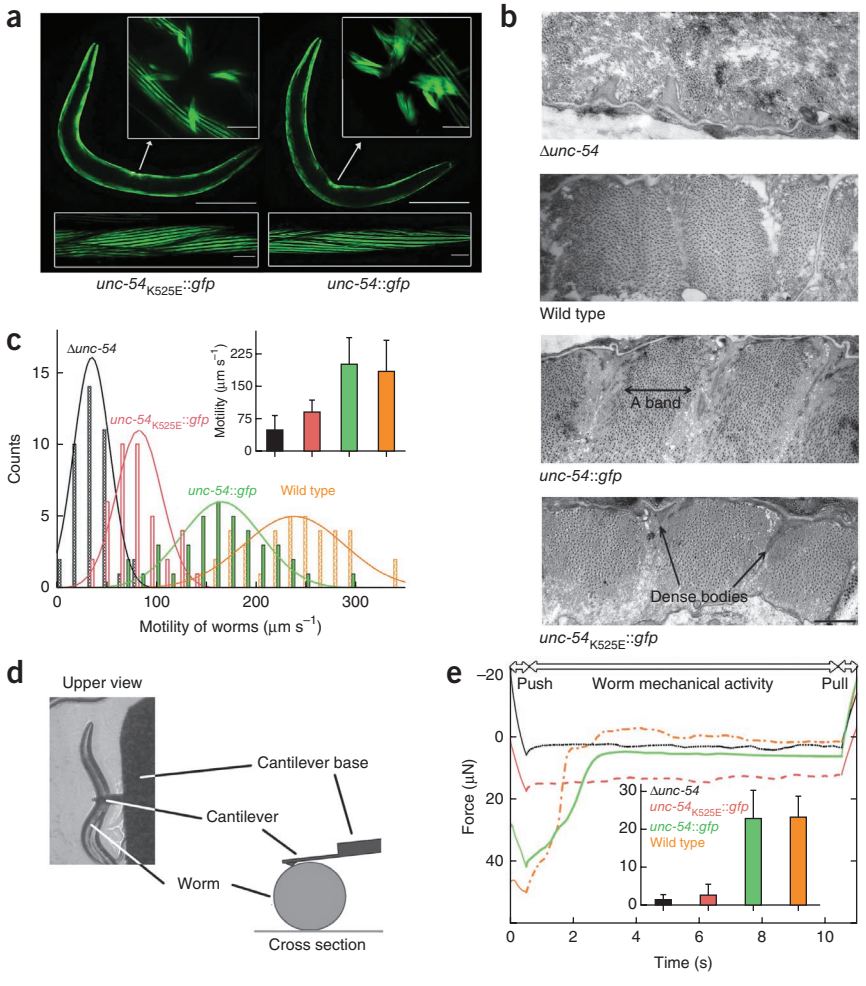

Figure 5 *C. elegans* bearing a loss-of-function mutation in the activation loop show reduced mechanical efficiency and a reduced force-generating capability of myosin. (**a**) Worms from the Δ*unc-54*;*unc-54*::*gfp* (labeled here *unc-54*::*gfp*) and Δ*unc-54*;*unc-54*$_{K525E}$::*gfp* (labeled here *unc-54*$_{K525E}$::*gfp*) strains visualized by confocal microscopy using GFP fluorescence (scale bars, 200 μm). UNC-54::GFP and UNC-54$_{K525E}$::GFP are also expressed in vulval muscle cells that are responsible for egg production and are localized on the ventral side of the body (scale bars, upper insets, 10 μm). In the lower inset, the parallel A bands of a single spindle-shaped body-wall muscle cell are visualized (scale bars, lower insets, 10 μm). (**b**) Electron microscopy of cross sections of the body-wall muscle of adult *C. elegans* worms. Scale bar, 500 nm. (**c**) Distribution of the motility of *C. elegans* worms with the wild-type, Δ*unc-54*, *unc-54*::*gfp* or *unc-54*$_{K525E}$::*gfp* genetic background. The inset shows the average velocities of the worms from each of the four strains after treatment with FUDR. Error bars, s.d. of at least three independent experiments. (**d**) Schematic of force-measuring experiments, applied by AFM. (**e**) Typical force curves produced by the four *C. elegans* strains examined during the force-measuring experiments. Worms were exposed to a deforming force (push), and their force-generating activities were measured (worm mechanical activity) until the retraction of the cantilever (pull). The inset shows the force production averages and error bars with s.d. of 15–25 worms from each strain.

myo-4 are expressed in the body-wall muscle. Whereas *myo-3* encodes a minor isoform that is essential for the formation of thick filaments[38], *myo-4*, also called *unc-54*, codes for a protein that is the major component of the body-wall muscle and is mainly responsible for evoking body movement[39]. *C. elegans* mutant strains defective for UNC-54 are paralyzed (meaning that they have an uncoordinated phenotype), and the speed of their movement is 20% of the speed of the wild-type *C. elegans* worms. Previous studies reported that the applied *C. elegans* strain with a substitution in the e1092 allele does not express myosin heavy chain B (MHC-B)[40], and the introduction of *unc-54* into this strain partially rescued the motility of the worms[41].

First, we restored the body-wall muscle function of *unc-54*–null mutant (Δ*unc-54*) worms[40] using a transgenically introduced, GFP-labeled *unc-54* gene (p*unc-54*::UNC-54::GFP plasmid construct, and the resulting myosin-GFP chimera protein is called UNC-54::GFP). To test how the activation-loop–specific mutation that is responsible for the inability of actin to activate myosin affects muscle functions and worm movement, we generated a mutant version of this construct, p*unc-54*::UNC-54$_{K525E}$::GFP, in which we replaced the genetic code of Lys525 (the *C. elegans* homolog to *D. discoideum* Arg520) with that of glutamate (creating the K525E mutation). We compared the physiological properties of the strains Δ*unc-54*;*unc-54*::*gfp* (containing UNC-54::GFP) and Δ*unc-54*; *unc-54*$_{K525E}$::*gfp* (containing UNC-54$_{K525E}$::GFP) to those of the wild-type (N2) and Δ*unc-54* strains. The gross anatomical features (body size and morphology) and vial parameters (lifespan and larval development) were similar in each strain (**Supplementary Fig. 2** and **Supplementary Table 1a**,**b**).

Transgenic worms expressing UNC-54::GFP or UNC-54$_{K525E}$::GFP showed intact fiber and obliquely striated sarcomere structures of the body-wall muscles along their entire bodies, as revealed by confocal and transmission electron microscopy, respectively (**Fig. 5a**,**b**). By contrast, Δ*unc-54* worms had a stunted, disorganized sarcomere structure because they lacked the major myo-4 isoform.

We investigated motile function by measuring the velocities of the worms' tails in video recordings using custom-written image-processing routines. We compared the movement parameters of wild-type, Δ*unc-54*, Δ*unc-54*;*unc-54*::*gfp* and Δ*unc-54*;*unc-54*$_{K525E}$::*gfp* strains using a real-time automatic movement analyzer (δVision). The reduced motility of the Δ*unc-54* worms was restored (71% restoration, $n = 20$) by introducing the wild-type copy of *unc-54* (producing the Δ*unc-54*; *unc-54*::*gfp* strain) (**Fig. 5c**). This amount of restoration of motile function is similar to that seen by researchers in a previous study[41]. However, there are several possible reasons why the Δ*unc-54*; *unc-54*::*gfp* strain has reduced motility compared to wild-type worms, including the possibility that the GFP-tagged myosin is not expressed at the same level as wild-type myosin or that the tagged protein is not incorporated into thick filaments as efficiently as the endogenous myosin. We compared the expression levels of body-wall myosin that we detected using the fluorescence of the attached GFP in transgenic worms and found no correlation of these expression levels with the speed of the worms (**Supplementary Table 1c**). Worms from the Δ*unc-54*;*unc-54*$_{K525E}$::*gfp* strain moved markedly slower than wild-type worms but moved 2.2 times faster than Δ*unc-54* worms. We also studied the movement of worms treated with 5-fluoro-2′-deoxyuridine (floxuridine, or FUDR), which inhibits egg production. After treatment with FUDR, there was a complete restoration of speed in the Δ*unc-54*;*unc-54*::*gfp* worms (**Fig. 5c**, inset). In terms of the activation-loop–mutant myosin (in the Δ*unc-54*;*unc-54*$_{K525E}$::*gfp* strain), a two-fold difference in speed remained between the activation-loop–mutant strain and the Δ*unc-54* strain. In summary, blocking actin activation by introducing an activation-loop mutation in myosin reduces but does not abolish the speed of the worms (**Supplementary Movie 1**).

To investigate the effect of the activation-loop mutation on the *in vivo* force generation of body-wall muscles, we devised new experimental procedures using atomic force microscopy (AFM) (**Fig. 5d**). We estimated the force generated actively by the worms by characterizing the mechanical response of the worms evoked by pushing them with a cantilever. Perturbating worms with the cantilever evoked an escape response, the vigor of which seemed to correlate with myosin type. This escape response consisted of oscillatory contractions, leading to a final escape of the worm from underneath the AFM cantilever. The magnitude of the force response was measured in time-dependent force traces (**Fig. 5e**). The mean force values were ~20 times greater in the wild-type and Δ*unc-54*; *unc-54*::*gfp* worms than in the Δ*unc-54* and Δ*unc-54*;*unc-54*$_{K525E}$::*gfp* worms (**Fig. 5e**, inset). Activation-loop–mutant worms were only slightly stronger than those worms without UNC-54 body-wall myosin ($P = 0.1563$, $n = 24$; **Supplementary Movie 2**).

In summary, mutational depletion of actin activation of myosin drastically weakens muscle contraction despite the unloaded motile functions that are retained. These findings are consistent with our biochemical and *in vitro* motility assay results, which showed that actin activation increases the ratio of effective to futile actomyosin cycles; however, actin-filament sliding is retained by the small number of mechanically cycling myosin heads.

DISCUSSION

Despite several decades of intense investigation[42], the structural mechanism underlying actin activation of myosin and its functional role were unknown until now. We have found a previously unidentified actin-binding region of myosin called the activation loop, which is specifically responsible for the actin activation process. This highly conserved loop interacts with the N-terminal peptide segment of actin, promoting efficient force generation.

Structural mechanism of actin activation

The structural location of the activation loop suggests a mechanism in which actin binding activates the lever swing. The activation loop is located in the upper helix of the relay region, which is structurally coupled with the converter and lever regions (**Figs. 1b**, **2** and **Supplementary Fig. 1**). Comparing the lever-down and lever-up structures of myosin, the N terminus of the relay helix and the activation loop move together at switch 2 loop closure. According to structural models, the movement of switch 2, and possibly the central β-sheet core of myosin, initiates the lever swing by pulling the N-terminal segment of the relay helix[5,43,44]. This structural model for recovery and powerstroke swings is called the seesaw mechanism[43,45]. Actin binding to the activation loop of the upper relay region may tilt this structural complex and increase the probability of the lever swing at the initiation of the powerstroke.

Although the activation loop is a conserved structural element of myosin, its sequence may vary among different types of myosins, with the exception of the positively charged amino acid side chain at the tip of the loop in all myosins (Arg520 in *D. discoideum* myosin) (**Supplementary Fig. 1**). Actin activation is tuned by the length of the activation loop, as was recently reported[18]. When the sequence of the activation loop of smooth-muscle myosin was replaced with that of the skeletal-muscle myosin, the actin-activated ATPase activity increased by two-fold, whereas the unloaded actin-sliding velocity did not change substantially[18]. Through this mechanism, the ratio of the working myosin heads are tuned to adapt features of different myosins to their physiological functions.

Allosteric regulation by kinetic pathway selection

Actin activation is a specific type of allosteric regulation in which the relative flux of the favored pathway is increased compared to the unfavored pathway by accelerating the rate-limiting step. For a 100-fold increase in the rate constant, only a small (10 kJ mol^{-1}) decrease in the energy barrier is required. This small change in the energetic landscape results in an increase of two orders of magnitude in the efficiency of the actomyosin powerstroke by the kinetic pathway selection mechanism[6]. Another type of allosteric regulation is common among metabolic enzymes when the favored pathway is selected by the binding of a regulator ligand, which shifts the equilibrium between the active and inactive enzyme populations (known as thermodynamic pathway selection).

The importance of the mechanism underlying kinetic pathway selection in actin activation regulated by the activation loop is highlighted by the fact that despite functionally important differences in the structure and kinetic properties of the myosin isoforms, they share this common mechanistic framework. In addition, mechanistic knowledge regarding actin activation of myosin also helps us understand why allosteric activation is a general mechanism in the P-loop NTPase family, which includes kinesins, dyneins, DNA and RNA polymerases, initiation and elongation factors in ribosomal translation and signaling enzyme complexes. For DNA polymerases, when the correct Watson-Crick geometry is formed, the orientation of the DNA activates a rate-limiting conformational change that induces a chemical displacement of the nucleotide[46]. This effect provides extraordinary fidelity during replication. Translation factors also provide high fidelity for protein synthesis through the kinetic pathway selection mechanism. When the cognate codon-anticodon complex is formed, the elongation factor Tu aminoacyl-tRNA complex is allosterically activated, inducing aminoacyl-tRNA transfer and peptide bond formation[47]. The signal recognition particle (SRP54) also goes through a conformational change at receptor binding, activating GTP hydrolysis and translocation of the cargo protein through the endoplasmic reticulum[48]. Regardless of how clear these examples seem, the identical nature of the mechanisms that support the high efficiency of the productive complexes has not been recognized.

In summary, similar track and effector protein activations are evolutionarily conserved general processes among P-loop NTPases. In motor and signaling enzyme systems, the track or activator interactions channel the enzyme processes into effective working cycles. The similarity of these mechanisms may reflect similar structural backgrounds, which would reveal further general and evolutionary conserved functions of this enzyme family.

METHODS

Methods and any associated references are available in the online version of the paper at http://www.nature.com/nsmb/.

Note: Supplementary information is available on the Nature Structural & Molecular Biology website.

ACKNOWLEDGMENTS

We thank A.G. Szent-Györgyi, C.R. Bagshaw and M. Kovács for insightful discussions and helpful comments. We thank E. Málnási-Csizmadia for the processing of videos. This work was supported by the European Research Council (European Community's Seventh Framework Programme (FP7/2007-2013)/European Research Council grant agreement no. 208319), the European Union in collaboration with the European Social Fund (grant agreement no. TAMOP-4.2.1/B-09/1/KMR), the National Office for Research and Technology and the European Union (European Regional Development Fund), under the sponsorship of the National Technology Programme (NTP TECH_08_A1/2-2008-0106). T.V. is a grantee of the János Bolyai scholarship.

AUTHOR CONTRIBUTIONS

B.H.V. and A.M.-C. designed, conducted and analyzed all experiments and wrote the paper. Z.Y. conducted the *in silico* experiments. B.K. designed experiments and contributed to the writing of the paper. T.V. and P.E. contributed to the *C. elegans* experiments. I.B.-N. contributed to the *in vitro* motility experiments. A.L.K. carried out electron microscopy. M.K. designed and conducted the AFM experiment. P.H. designed the analysis of the movement of *C. elegans*.

COMPETING FINANCIAL INTERESTS

The authors declare no competing financial interests.

Published online at http://www.nature.com/nsmb/.
Reprints and permissions information is available online at http://www.nature.com/reprints/index.html.

1. Pollard, T.D. Reflections on a quarter century of research on contractile systems. *Trends Biochem. Sci.* **25**, 607–611 (2000).
2. Sweeney, H.L. & Houdusse, A. Structural and functional insights into the Myosin motor mechanism. *Annu. Rev. Biophys.* **39**, 539–557 (2010).
3. Odronitz, F. & Kollmar, M. Drawing the tree of eukaryotic life based on the analysis of 2,269 manually annotated myosins from 328 species. *Genome Biol.* **8**, R196 (2007).
4. Bauer, C.B., Holden, H.M., Thoden, J.B., Smith, R. & Rayment, I. X-ray structures of the apo and MgATP-bound states of *Dictyostelium discoideum* myosin motor domain. *J. Biol. Chem.* **275**, 38494–38499 (2000).
5. Gyimesi, M. *et al.* The mechanism of the reverse recovery step, phosphate release, and actin activation of *Dictyostelium* myosin II. *J. Biol. Chem.* **283**, 8153–8163 (2008).
6. Málnási-Csizmadia, A. & Kovacs, M. Emerging complex pathways of the actomyosin powerstroke. *Trends Biochem. Sci.* **35**, 684–690 (2010).
7. Goody, R.S. & Hofmann-Goody, W. Exchange factors, effectors, GAPs and motor proteins: common thermodynamic and kinetic principles for different functions. *Eur. Biophys. J.* **31**, 268–274 (2002).
8. Bhattacharyya, R.P. *et al.* The Ste5 scaffold allosterically modulates signaling output of the yeast mating pathway. *Science* **311**, 822–826 (2006).
9. Holmes, K.C., Angert, I., Kull, F.J., Jahn, W. & Schroder, R.R. Electron cryo-microscopy shows how strong binding of myosin to actin releases nucleotide. *Nature* **425**, 423–427 (2003).
10. Oda, T., Iwasa, M., Aihara, T., Maeda, Y. & Narita, A. The nature of the globular- to fibrous-actin transition. *Nature* **457**, 441–445 (2009).
11. Holmes, K.C., Schroder, R.R., Sweeney, H.L. & Houdusse, A. The structure of the rigor complex and its implications for the power stroke. *Phil. Trans. R. Soc. Lond. B* **359**, 1819–1828 (2004).
12. Lorenz, M. & Holmes, K.C. The actin-myosin interface. *Proc. Natl. Acad. Sci. USA* **107**, 12529–12534 (2010).
13. Liu, Y., Scolari, M., Im, W. & Woo, H.J. Protein-protein interactions in actin-myosin binding and structural effects of R405Q mutation: a molecular dynamics study. *Proteins* **64**, 156–166 (2006).
14. Root, D.D. A computational comparison of the atomic models of the actomyosin interface. *Cell Biochem. Biophys.* **37**, 97–110 (2002).
15. Kintses, B. *et al.* Reversible movement of switch 1 loop of myosin determines actin interaction. *EMBO J.* **26**, 265–274 (2007).
16. Sasaki, N., Asukagawa, H., Yasuda, R., Hiratsuka, T. & Sutoh, K. Deletion of the myopathy loop of *Dictyostelium* myosin II and its impact on motor functions. *J. Biol. Chem.* **274**, 37840–37844 (1999).
17. Gyimesi, M., Tsaturyan, A.K., Kellermayer, M.S. & Malnasi-Csizmadia, A. Kinetic characterization of the function of myosin loop 4 in the actin-myosin interaction. *Biochemistry* **47**, 283–291 (2008).
18. Kojima, S. *et al.* Functional roles of ionic and hydrophobic surface loops in smooth muscle myosin: their interactions with actin. *Biochemistry* **40**, 657–664 (2001).
19. Onishi, H., Mikhailenko, S.V. & Morales, M.F. Toward understanding actin activation of myosin ATPase: the role of myosin surface loops. *Proc. Natl. Acad. Sci. USA* **103**, 6136–6141 (2006).
20. Furch, M., Remmel, B., Geeves, M.A. & Manstein, D.J. Stabilization of the actomyosin complex by negative charges on myosin. *Biochemistry* **39**, 11602–11608 (2000).
21. Joel, P.B., Trybus, K.M. & Sweeney, H.L. Two conserved lysines at the 50/20-kDa junction of myosin are necessary for triggering actin activation. *J. Biol. Chem.* **276**, 2998–3003 (2001).
22. Miller, C.J., Wong, W.W., Bobkova, E., Rubenstein, P.A. & Reisler, E. Mutational analysis of the role of the N terminus of actin in actomyosin interactions. Comparison with other mutant actins and implications for the cross-bridge cycle. *Biochemistry* **35**, 16557–16565 (1996).
23. Gu, J., Xu, S. & Yu, L.C. A model of cross-bridge attachment to actin in the A*M*ATP state based on X-ray diffraction from permeabilized rabbit psoas muscle. *Biophys. J.* **82**, 2123–2133 (2002).
24. Sutoh, K. Mapping of actin-binding sites on the heavy chain of myosin subfragment 1. *Biochemistry* **22**, 1579–1585 (1983).
25. Andreev, O.A. & Reshetnyak, Y.K. Mechanism of formation of actomyosin interface. *J. Mol. Biol.* **365**, 551–554 (2007).

26. Van Dijk, J. *et al.* Differences in the ionic interaction of actin with the motor domains of nonmuscle and muscle myosin II. *Eur. J. Biochem.* **260**, 672–683 (1999).
27. Jahn, W. The association of actin and myosin in the presence of γ-amido-ATP proceeds mainly via a complex with myosin in the closed conformation. *Biochemistry* **46**, 9654–9664 (2007).
28. Wray, J. & Jahn, W. γ-amido-ATP stabilizes a high-fluorescence state of myosin subfragment 1. *FEBS Lett.* **518**, 97–100 (2002).
29. Málnási-Csizmadia, A. *et al.* Kinetic resolution of a conformational transition and the ATP hydrolysis step using relaxation methods with a *Dictyostelium* myosin II mutant containing a single tryptophan residue. *Biochemistry* **40**, 12727–12737 (2001).
30. Cooke, R., White, H. & Pate, E. A model of the release of myosin heads from actin in rapidly contracting muscle fibers. *Biophys. J.* **66**, 778–788 (1994).
31. Nyitrai, M. *et al.* What limits the velocity of fast-skeletal muscle contraction in mammals? *J. Mol. Biol.* **355**, 432–442 (2006).
32. Purcell, T.J. *et al.* Nucleotide pocket thermodynamics measured by EPR reveal how energy partitioning relates myosin speed to efficiency. *J. Mol. Biol.* **407**, 79–91 (2011).
33. Forgacs, E. *et al.* Switch 1 mutation S217A converts myosin V into a low duty ratio motor. *J. Biol. Chem.* **284**, 2138–2149 (2009).
34. Lin, T., Greenberg, M.J., Moore, J.R. & Ostap, E.M. A hearing loss-associated myo1c mutation (R156W) decreases the myosin duty ratio and force sensitivity. *Biochemistry* **50**, 1831–1838 (2011).
35. Nagy, N.T. *et al.* Functional adaptation of the switch-2 nucleotide sensor enables rapid processive translocation by myosin-5. *FASEB J.* **24**, 4480–4490 (2010).
36. Takács, B. *et al.* Myosin cleft closure determines the energetics of the actomyosin interaction. *FASEB J.* **25**, 111–121 (2011).
37. Uyeda, T.Q., Abramson, P.D. & Spudich, J.A. The neck region of the myosin motor domain acts as a lever arm to generate movement. *Proc. Natl. Acad. Sci. USA* **93**, 4459–4464 (1996).
38. Waterston, R.H. The minor myosin heavy chain, mhcA, of *Caenorhabditis elegans* is necessary for the initiation of thick filament assembly. *EMBO J.* **8**, 3429–3436 (1989).
39. Moerman, D.G., Plurad, S., Waterston, R.H. & Baillie, D.L. Mutations in the unc-54 myosin heavy chain gene of *Caenorhabditis elegans* that alter contractility but not muscle structure. *Cell* **29**, 773–781 (1982).
40. Anderson, P. & Brenner, S. A selection for myosin heavy chain mutants in the nematode *Caenorhabditis elegans*. *Proc. Natl. Acad. Sci. USA* **81**, 4470–4474 (1984).
41. Fire, A. & Waterston, R.H. Proper expression of myosin genes in transgenic nematodes. *EMBO J.* **8**, 3419–3428 (1989).
42. Biro, N.A. & Szent-Gyorgyi, A.E. The effect of actin and physico-chemical changes on the myosin ATP-ase system, and on washed muscle. *Hung. Acta Physiol.* **2**, 120–133 (1949).
43. Fischer, S., Windshugel, B., Horak, D., Holmes, K.C. & Smith, J.C. Structural mechanism of the recovery stroke in the myosin molecular motor. *Proc. Natl. Acad. Sci. USA* **102**, 6873–6878 (2005).
44. Yu, H., Ma, L., Yang, Y. & Cui, Q. Mechanochemical coupling in the myosin motor domain. I. Insights from equilibrium active-site simulations. *PLoS Comput. Biol.* **3**, e21 (2007).
45. Kintses, B., Yang, Z. & Malnasi-Csizmadia, A. Experimental investigation of the seesaw mechanism of the relay region that moves the myosin lever arm. *J. Biol. Chem.* **283**, 34121–34128 (2008).
46. Johnson, K.A. Conformational coupling in DNA polymerase fidelity. *Annu. Rev. Biochem.* **62**, 685–713 (1993).
47. Gromadski, K.B. & Rodnina, M.V. Kinetic determinants of high-fidelity tRNA discrimination on the ribosome. *Mol. Cell* **13**, 191–200 (2004).
48. Egea, P.F. *et al.* Substrate twinning activates the signal recognition particle and its receptor. *Nature* **427**, 215–221 (2004).

ONLINE METHODS

Expression and purification of proteins. The R520E, Δ519–523, R520Q and R520K mutations were introduced into the *D. discoideum* myosin 2 motor domain. Proteins were expressed in *D. discoideum* AX2-ORF$^+$ cells and then isolated using histidine-tagged affinity chromatography as previously described[49]. Proteins were dialyzed against assay buffer. *M. musculus* wild-type and K502E myosin 5a S1 constructs were expressed in an Sf9 baculovirus system and purified as described previously[50]. The expressed proteins also were extended with an N-terminal GFP and C-terminal Flag-tag. Proteins were dialyzed against assay buffer 2. For details regarding cloning and buffers, see **Supplementary Methods**.

Preparation, purification and pyrene-labeling of actin was carried out as described[51,52]. Actin filaments were stabilized using a 1.5-fold molar excess of phalloidin (Molecular Probes).

For the strains and genetics of *C. elegans* see **Supplementary Methods**.

Actomyosin covalent cross-linking by EDC. A 30 μM *D. discoideum* motor domain construct (either wild type or R520K) was mixed with 60 μM F-actin in assay buffer, and 5 mM EDC (Fluka) was added to initiate the zero-length crosslinking reaction at 20 °C. The reaction was terminated with 10 mM β-mercapto-ethanol, and the cross-linked products were analyzed by SDS-PAGE (with a 5–15% gradient minigel) using a Pharmacia Biotech Phast system.

Transient kinetic measurements. Stopped-flow measurements were carried out using a BioLogic SF 300 apparatus equipped with 200 W Super-Quiet Mercury-Xenon lamps (Hamamatsu Photonics). All experiments were carried out at 20 °C in assay buffer. The means ± s.d. of the observed rate constants k_{obs} from three independent experiments were plotted as a function of concentration. Plot fitting and data analyses were conducted using Biokine and OriginLab 7.5. For details regarding the experimental conditions and for a detailed analysis of the data, see **Supplementary Methods**.

Actin co-sedimentation assay. Samples of 2 μM *D. discoideum* myosin motor domain in the presence of 2 mM ATP and increasing amounts of F-actin (0–130 μM) were ultracentrifuged at 350,000*g* for 20 min at 4 °C. The resulting supernatants at each concentration of actin were collected, and the pellets were dissolved in the same volume of buffer (1 mM HEPES, 2 mM $MgCl_2$ and 1 mM DTT, pH 7.2) as the volume of the appropriate supernatants. After SDS-PAGE, a densitometric method was used to detect the amount of myosin in the pellets and supernatants, and the fractional actin attachment of myosin at each actin concentration was determined (calculated as the volume of the pellet over the volume of the pellet plus the supernatant). Myosin without actin or ATP was used as a control (resulting in no myosin in the pellet), and 2 μM myosin with 40 μM actin and no ATP was used as a second control (resulting in all the myosin being in complex with actin in the pellet). Before the assay, nonfunctional myosin heads were eliminated by ultracentrifugation with actin in the presence of 5 mM ATP.

Physiological and motility assays of *C. elegans*. All assays were carried out at 25 °C with synchronized *C. elegans* cultures. For the FUDR-treated motility assays, the worms were maintained at 20 °C until the L4 larval stage and were then transferred to nematode growth media plates supplemented with 300 mg ml^{-1} FUDR for 1 d. Sterile adult worms were then transferred to the assay plates. Twenty worms from each strain were recorded every 24 h from the young adult stage until death. Worms were considered dead when they stopped pharyngeal pumping and stopped responding to touching. For the FUDR-untreated motility assay, the worms were maintained at 20 °C until the second day of their adult stage, and 40 worms from each strain were recorded. Nematodes were tapped with a glass rod to evoke motion, and δVision software was used for tracking the movement and the tail velocity of the worms.

Atomic force microscopy. Individual *C. elegans* worms on an agarose plate were mechanically manipulated with an AsylumResearch MFP3D atomic force microscope. Olympus AC160 cantilevers were used, which were calibrated using the thermal method[53]. In the cantilever assay, the worms were exposed to an average initial force of 30 μN. Then, the change in force was monitored as a function of time for a period of 10 s. To quantify the vigor in the force response, the differences between the initial force and the force after 10 s were calculated and visualized. The difference in the *y* intercepts of the curves was the result of a shift between the curves present for display purposes. Experiments were carried out at 25 °C. Data were analyzed using Igor Pro 6.04.

Additional methods. Detailed descriptions of actin-activated ATPase measurements, *in vitro* motility assays, microparticle bombardment, confocal microscopy and simulations of molecular dynamics are available in **Supplementary Methods**.

49. Málnási-Csizmadia, A., Woolley, R.J. & Bagshaw, C.R. Resolution of conformational states of *Dictyostelium* myosin II motor domain using tryptophan (W501) mutants: implications for the open-closed transition identified by crystallography. *Biochemistry* **39**, 16135–16146 (2000).
50. Yang, Y., Kovacs, M., Xu, Q., Anderson, J.B. & Sellers, J.R. Myosin VIIB from *Drosophila* is a high duty ratio motor. *J. Biol. Chem.* **280**, 32061–32068 (2005).
51. Pardee, J.D. & Spudich, J.A. Purification of muscle actin. *Methods Cell Biol.* **24**, 271–289 (1982).
52. Cooper, J.A., Walker, S.B. & Pollard, T.D. Pyrene actin: documentation of the validity of a sensitive assay for actin polymerization. *J. Muscle Res. Cell Motil.* **4**, 253–262 (1983).
53. Hutter, J.L. & Bechhoefer, J. Calibration of atomic-force microscope tips. *Rev. Sci. Instrum.* **64**, 1868–1873 (1993).